RADIATION RESEARCH **196**, 225–234 (2021)
0033-7587/21 $15.00

DOI: 10.1667/RADE-20-00025.1

High Relative Biological Effectiveness of 2 MeV Fast Neutrons for Induction of Medulloblastoma in *Ptch1*$^{+/-}$ Mice with Radiation-specific Deletion on Chromosome 13

Chizuru Tsuruoka,[a] Mutsumi Kaminishi,[a] Mayumi Shinagawa,[a] Yi Shang,[a] Yoshiko Amasaki,[a] Yoshiya Shimada[b] and Shizuko Kakinuma[a,1]

[a] *Department of Radiation Effects Research, National Institute of Radiological Sciences, National Institutes for Quantum and Radiological Science and Technology, Chiba, Japan; and* [b] *Institute for Environmental Science, Kamikita-gun, Aomori, Japan*

Tsuruoka, C., Kaminishi, M., Shinagawa, M., Shang, Y., Amasaki, Y., Shimada, Y. and Kakinuma, S. High Relative Biological Effectiveness of 2 MeV Fast Neutrons for Induction of Medulloblastoma in *Ptch1*$^{+/-}$ Mice with Radiation-specific Deletion on Chromosome 13. *Radiat. Res*. 196, 225–234 (2021).

Neutron radiation, a high-linear energy transfer radiation, has a high relative biological effectiveness (RBE) for various end points. The age at exposure is an important modifier of the effects of radiation, including carcinogenesis, with infants being generally more radiosensitive. *Ptch1*$^{+/-}$ mice offer a unique experimental system for assessing radiation carcinogenesis. Spontaneous development of medulloblastoma tumors occurs in nonirradiated animals that lose their *Ptch1*$^{+}$ allele, most frequently by a loss of heterozygosity (LOH) of chromosome 13 via recombination or non-disjunction (referred to as S-type tumors). In contrast, tumors occur in irradiated *Ptch1*$^{+/-}$ mice as a result of chromosome 13 LOH with an interstitial deletion (R-type), making spontaneous and radiation-induced tumors discernible. To elucidate the influence of age on the effect of fast neutrons, we irradiated *Ptch1*$^{+/-}$ mice with neutrons (mean energy, ~2 MeV) or γ rays on embryonic day (E)14 and E17 and on postnatal day (P)1, 4 or 10 and classified the resulting medulloblastomas based on chromosome 13 aberrations. Instead of LOH, some tumors harbored mutations in their *Ptch1*$^{+}$ gene via a nonirradiation-associated mechanism such as duplication, insertion, base substitution or deletion with microhomology-mediated end joining; thus, these tumors were classified as S-type. The RBE regarding the induction of R-type tumors was 12.9 (8.6, 17.2), 9.6 (6.9, 12.3), 21.5 (17.2, 25.8), and 7.1 (4.7, 9.5) (mean and 95% confidence interval) for mice irradiated on E14, E17, P1 and P4, respectively, with the highest value seen during the most active development of the tissue and P10 being completely resistant. These results indicate that the developmental stage at exposure of the tissue influences the RBE of neutrons.

INTRODUCTION

Human exposure to neutron radiation is increasing with the development of new technologies. For example, astronauts are exposed to neutrons produced from protons impinging on spacecraft, cancer patients are exposed to secondary neutrons generated in therapeutic devices related to proton, heavy-particle and intensity modulated radiation therapies, and people have been exposed to neutrons as a result of severe nuclear accidents (*1–5*). Neutron radiation is a high-linear energy transfer (LET) values compared to gamma (γ) rays, its relative biological effectiveness (RBE) is high for biological end points including those assessed *in vitro* and *in vivo*, such as cell killing, life shortening or tumor development (*6–9*). The age at the time of exposure is an important modifier of various radiation effects including tumor induction (*10*). The recent development of proton and carbon-ion radiotherapies as treatments for pediatric cancer (*11, 12*) has raised substantial concerns regarding neutron-induced second-cancer risk in survivors who have received these therapies (*13–16*). Epidemiology on the carcinogenic effect of neutrons has been very limited with few exceptions (*17*). Regarding the effect of radiation exposure during infancy, the result of the atomic bomb survivor cohort with *in utero*/childhood exposure has been among the most informative (*18*), but neutrons were only a small component of the overall exposure. On the other hand, rodent experiments exploring the long-term consequences of neutron exposure during infancy have indicated its significant effects on life span and tumor induction (*19–21*). Still, extremely limited data have been available on the carcinogenic effect of neutron radiation during infancy.

Cancer develops as a result of various environmental and genetic factors including radiation exposure (*22*). Cancer-

Editor's note. The online version of this article (DOI: https://doi.org/10.1667/RADE-21-00025.1) contains supplementary information that is available to all authorized users.

[1] Address for correspondence: 4-9-1 Anagawa, Inage-ku, Chiba 263-8555, Japan; email: kakinuma.shizuko@qst.go.jp.

prone subpopulations include individuals who have genetic defects in DNA repair machinery or in signaling pathways related to organ development, examples of the latter being the Hedgehog and Wnt cascades (*23*). Among the mouse models based on deficiencies in these genes is the *Ptch1*$^{+/-}$ mouse, a model of Gorlin syndrome, which carries a defective copy of a tumor suppressor gene involved in negative regulation of the sonic hedgehog (Shh) signaling pathway (*24*). *Ptch1*$^{+/-}$ mice often develop medulloblastomas (MBs) as a result of deregulation of the Shh signal in the granule cells of the external granular layer of the cerebellum (*25*), and the frequency increases after mice are exposed to radiation during a narrow window of time around birth (*26*). Loss of the wild-type *Ptch1* allele on chromosome 13 is evident in almost all spontaneously developed and radiation-induced MBs (*27*). We previously confirmed that the MBs which developed after radiation exposure exhibited an interstitial deletion resulting in loss of the wild-type *Ptch1* allele (designated as ''radiation-induced'' or R-type MB), and that almost all spontaneously developed MBs exhibited loss of all chromosomal regions distal to the wild-type *Ptch1* (designated as ''spontaneous'' or S-type MB) (*28, 29*). As such, MBs of *Ptch1*$^{+/-}$ mice provide a useful experimental system for directly assessing the cancer-inducing effect of radiation by focusing on these R-type tumors.

The goal of the current study was to clarify the age dependence of the effect of fast neutrons and their RBE regarding the induction of MBs in *Ptch1*$^{+/-}$ mice. For this purpose, we took advantage of the above-mentioned characteristics of genetic aberration specific to radiation-induced MBs. Furthermore, molecular analysis of the neutron-induced tumors revealed a complex biological mechanism distinct from that induced by γ rays and X rays.

MATERIALS AND METHODS

Mice

Mice having one nonfunctional *Ptch1* allele (*Ptch1*$^{tm1Zim/Cnrm}$, hereafter referred to as *Ptch1*$^{+/-}$), generated through disruption of exons 6 and 7 in 129Sv embryonic stem cells (*24*), were initially obtained from the European Mouse Mutation Archive (ID: EM:00159) (*30*), and were maintained on the C57BL/6JCrl (B6) background at the National Institute of Radiological Sciences, National Institutes for Quantum and Radiological Science and Technology (QST-NIRS; Chiba, Japan). F1 hybrid mice were generated by crossing wild-type C3H/HeNCrlCrlj (C3H) female and *Ptch1*$^{+/-}$ B6 males. Genotyping of mice was performed by polymerase chain reaction (PCR) of DNA isolated from ear punches as described elsewhere (*29*). The rearing environment was as described elsewhere (*29*). These experiments were carried out with permission from and under the regulation of the Institutional Animal Care and Use Committee of QST-NIRS (approval no. 11-1026).

Irradiations

Neutron irradiation was performed using the Neutron-exposure Accelerator System for Biological Effect Experiments (NASBEE) at QST-NIRS. This irradiation facility and related dosimetry have been described elsewhere (*31*). Briefly, homogeneous space distribution of neutrons over a diameter of 30 cm was confirmed by measurement using an ion chamber and a low-pressure proportional counter at several distances from the beam center. The ion chamber had been calibrated using a national standard traceable ^{60}Co photon source. The neutrons in the irradiation compartment have a mean energy of 2.3 MeV and are delivered at an average dose rate of 24 mGy/min (except that irradiation at 0.025 Gy was carried out at ~12 mGy/min), whereas the kerma of tissue-equivalent-plastic (A-150)-weighted mean energy was 3.0 MeV; the γ-ray contamination in the neutron beam was reduced to 18% by a shutter installed at the beam port (*31*). Mice received whole-body irradiation *in utero* on embryonic day (E)14 or E17 or on postnatal day (P)1, P4 or P10 with 0.025–0.5 Gy of neutrons. Perinatal mice in this study were therefore of both sexes. Gamma-ray irradiation was performed using a Gammacell® 40 (MDS Nordion™ Inc., Ottawa, Canada) with a ^{137}Cs source at a dose rate of 540 mGy/min. Non-anesthetized animals were put in an acrylic irradiation enclosure (diameter, 23 cm) during irradiation. Newborn mice (P1 and P4) were warmed by a halogen lamp after irradiation and were immediately returned to their mothers. To preserve animal numbers, historical nonirradiated and γ-ray irradiated groups (0.1 Gy and 0.5 Gy; E14, E17, P1 and P4) from our previously published study (*29*) were used with identical perinatal irradiation protocols. Control mice were not sham-irradiated. The experimental groups and animal numbers are shown in detail in Supplementary Table S1 (https://doi.org/10.1667/RADE-21-00025.1.S1).

Tissue Preparation and Analysis of MBs

After irradiation, mice were observed and tissue samples were prepared as described elsewhere (*29*). In brief, mice were observed daily and, upon moribundity, were euthanized under anesthesia for autopsy. Portions of cerebellar tumors and normal tissues (ear and tail) were snap frozen in liquid nitrogen. The remaining portions of brain and any other visible lesions were fixed in 10% phosphate-buffered formalin and used for pathological diagnosis using the system of the Japan StoreHouse of Animal Radiobiology Experiments (J-SHARE) (*32*).

LOH Analysis and Array-based Comparative Genomic Hybridization (CGH)

DNA preparation, LOH analysis and DNA copy number analysis were performed as described elsewhere (*27–29*). Briefly, LOH was analyzed for six microsatellite markers on chromosome 13 and a single-nucleotide polymorphism (SNP) in exon 23 of murine *Ptch1*. To examine DNA copy number aberrations affecting chromosome 13, array CGH analysis was performed using custom CGH microarrays (Agilent Technologies Inc., Santa Clara, CA; GEO Platform no. GPL19183). Fluorescent labeling of DNA, hybridization and post-hybridization washing were performed, and the array slides were processed and scanned following the manufacturer's protocol (Agilent Technologies Inc.). Probes with saturated signals were excluded, and then copy number variations were identified with Genomic Workbench Lite Edition 7.0 software (Agilent Technologies Inc.) using the probe-quality-weighted interval scores (ADM-2, threshold = 5.0) and default normalization and centralization of the data. The microarray data have been deposited in the Gene Expression Omnibus database under accession number GSE173641.

Mutation Analysis of Ptch1

PCR primers were designed to amplify four overlapping regions of *Ptch1* cDNA (exons 2–12, 11–19, 15–20, and 18–23; Supplementary Fig. S1A and Supplementary Table S2; https://doi.org/10.1667/RADE-21-00025.1.S1). To determine whether the mutation was on the B6 or C3H allele, we took advantage of the sequence of the *neo* cassette inserted in place of exons 6 and 7, as well as SNPs in *Ptch1* (Supplementary Fig. S1B and Supplementary Tables S2 and S3).

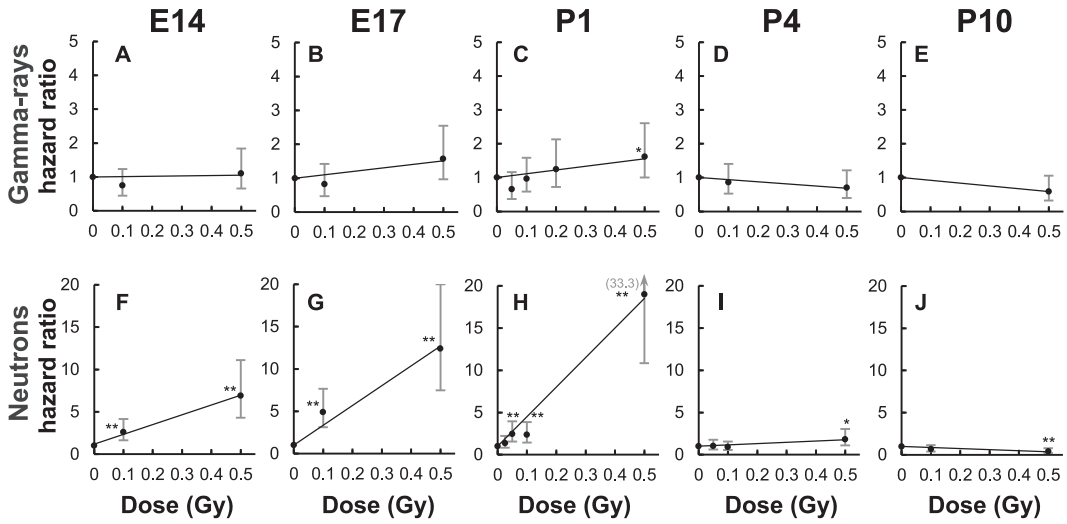

FIG. 1. Dose response of the hazard ratio of the incidence of medulloblastoma in *Ptch1*$^{+/-}$ mice. Panels A–J: *Ptch1*$^{+/-}$ mice received γ-ray (panels A–E) or fast neutron (panels F–J) irradiation on embryonic day (E)14 or 17 or postnatal day (P)1, 4 or 10 and were observed until P500. Data for groups γ-ray irradiated on E14 (0.1 and 0.5 Gy), E17 (0.1 and 0.5 Gy), P1 (0.1 and 0.5 Gy), and P4 (0.1 and 0.5 Gy) are from previously published work (*29*). Hazard ratios (dots) are superimposed with linear dose response models (solid line). Error bars show 95% confidence intervals; in panel H, the arrow with a number in parentheses indicates the upper limit. *$P < 0.05$ and **$P < 0.01$ by Cox regression.

Genomic DNA sequences were analyzed to determine mutations in the coding region and at the splice donor sites using the primers and PCR conditions as described elsewhere (Supplementary Fig. S1C and D, Supplementary Table S3).

Statistical Analysis

Pairwise differences in the incidence of the tumor types were evaluated from 2 × 2 contingency tables by Fisher's exact test. Cumulative incidence of MB-related moribundity was described using the Kaplan-Meier method, with difference between groups compared with the log-rank test. A Cox proportional hazards model was used to compute hazard ratios. For all analyses, $P < 0.05$ was considered significant. The relationship between the dose and hazard ratio was fitted to a linear equation with a *y*-intercept of 1 by the least-squares method. Given that RBE is generally defined as the ratio of the two radiation types that result in an identical effect, we defined it as the ratio of the slopes of the two radiation types. Standard errors of ratio values were calculated using the delta method. All statistical analyses were performed on StatMate V (ATMS, Chiba, Japan) and with software EZR (*33*).

RESULTS

Induction of MBs in Ptch1$^{+/-}$ *Mice after Gamma-Ray and Neutron Irradiation*

To clarify the biological effect of neutrons on the incidence of MB and its age dependence, compared to that of γ rays, we monitored the MB development up to P500 in *Ptch1*$^{+/-}$ mice that received neutron or γ-ray irradiation at 0.025–0.5 Gy. Moribundity was reached in 860 out of 1,291 mice (67%) by P500, and all MBs therein were pathologically diagnosed (Supplementary Table S1; https://doi.org/10.1667/RADE-21-00025.1.S1). Kaplan-Meier plots of MB-free survival were constructed using data before P500 (Supplementary Fig. S2), and a hazard ratio was calculated for each dose using the Cox proportional hazard model. Hazard ratios increased after neutron irradiation in a dose-dependent manner, where a significant increase was noted at lower doses of 0.1 Gy (E14 and E17, both $P < 0.01$) and 0.05 Gy (P1, $P < 0.01$); the susceptibility decreased slightly at P4 (with a significant increase only at 0.5 Gy, $P < 0.05$), whereas a significant reduction was observed at 0.5 Gy at P10 ($P < 0.01$) (Fig. 1). In contrast, the γ-ray irradiated groups showed a significant increase in the hazard ratio only for 0.5 Gy at P1 ($P < 0.05$), and there was only a non-significant increase for 0.5 Gy at E14 and E17, with a tendency toward a decrease at P4 and P10. Because of the small increase in the γ-ray irradiated groups, it was considered unrealistic to calculate a statistically significant RBE of neutrons as relative to that of γ rays based on these hazard ratio data.

LOH and DNA Copy Number Analyses of MB

As noted in the Introduction, MBs of *Ptch1*$^{+/-}$ mice are classified into two molecular subtypes, which R- and S-type, based on the pattern of LOH on chromosome 13 (*27, 28*). Therefore, we theorized that this technique would provide a more sensitive approach to obtaining the RBE of neutrons in the current study and identified R-type MBs to quantitatively compare the effects of neutrons and γ rays. We examined the LOH patterns of chromosome 13, which harbors the *Ptch1* locus, in all tumors from the experimental groups (nonirradiated, 31 tumors; neutron irradiated, 450 tumors; γ-ray irradiated, 292 tumors) except for one tumor and five tumors in the γ-ray and neutron irradiated groups, respectively, which were unavailable for

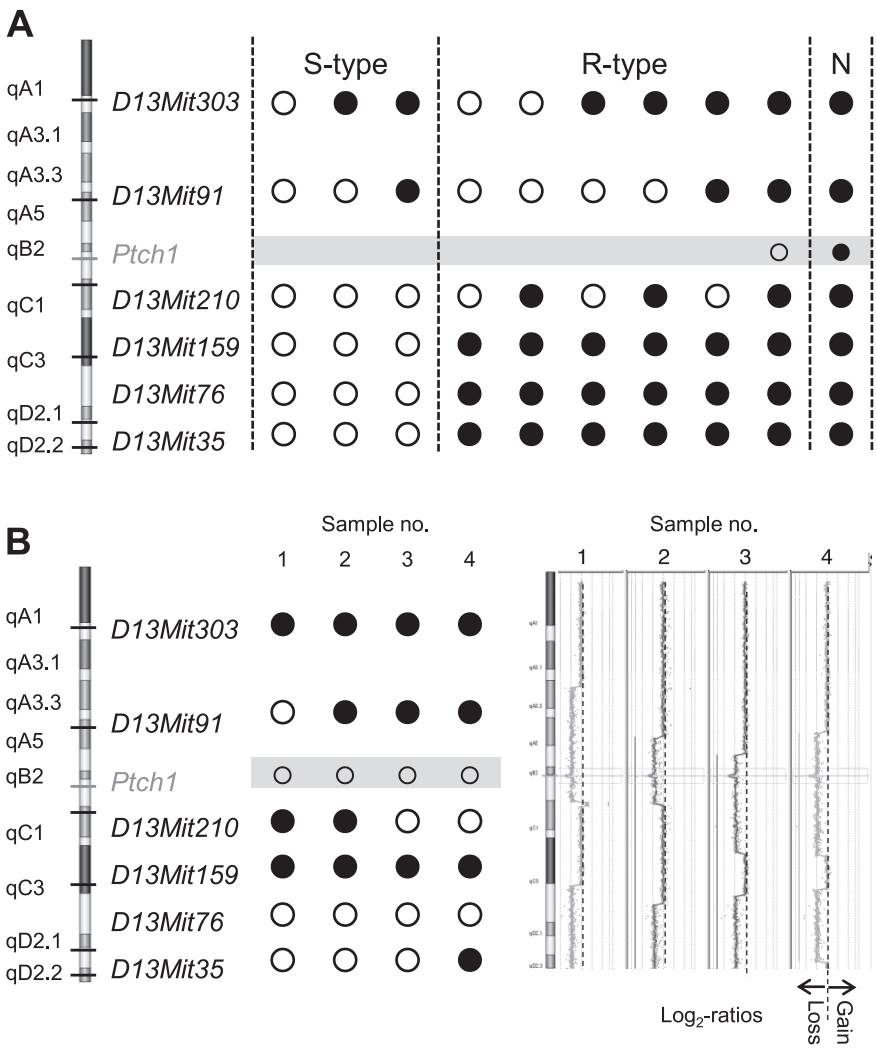

FIG. 2. Chromosome 13 loss of heterozygosity (LOH) and copy number aberrations in spontaneous and radiation-induced medulloblastomas from *Ptch1*$^{+/-}$ mice. Chromosomal regions and positions of polymorphic markers are shown on the left and right side of the schematic chromosome, respectively. Open circles indicate loss of a C3H allele, and filled circles indicate retention of both B6 and C3H alleles. Note that the wild-type *Ptch1* allele is located on the C3H chromosome in these mice. Large circles indicate the results of LOH obtained from polymorphic markers, and small circles indicate the results of LOH obtained from a single-nucleotide polymorphism (SNP) in exon 23 of *Ptch1*. Panel A: LOH patterns of S-type and R-type tumors. S-type tumors are marked by allelic losses at all consecutive markers distal to the *Ptch1* locus, indicated with gray shading, whereas R-type tumors show allelic loss(es) only at markers in the interstitial region around or within the *Ptch1* locus; N-type tumors were without LOH. Panel B, left side: LOH patterns of tumors with multiple deletions having a hemi-allelic loss at interstitial sites involving the *Ptch1* locus and another allelic loss at distal sites. LOH of these types existed only in neutron-induced MBs [0.5 Gy at P4 (sample no. 1), 0.1 Gy at P10 (no. 2 and 4), and 0.5 Gy at P10 (no. 3)]. Panel B, right side: Results of the DNA copy number analysis, indicating the consistency of these LOH patterns.

molecular analysis because of their autolysis. Almost all neutron- and γ-ray-induced MBs showed loss of the wild-type *Ptch1* allele on the C3H-derived copy of chromosome 13 and were classified as S- or R-type (Fig. 2A and Supplementary Fig. S3; https://doi.org/10.1667/RADE-21-00025.1.S1). Furthermore, the incidence of R-type MBs increased, whereas that of S-type MBs tended to decrease, in a dose-dependent manner in all groups except P10 (Fig. 3), as observed in a previously published study on X rays (*28*).

Interestingly, although rare, 5 of 305 (1.6%) R-type tumors in the neutron irradiated groups (one each from the group of 0.5 Gy at E14, P4 and P10 and two from 0.1 Gy at P10) exhibited two separate LOH regions of the C3H allele on chromosome 13, one encompassing the *Ptch1* locus and the other close to the telomere (Fig. 2B and Supplementary Fig. S3A; https://doi.org/10.1667/RADE-21-00025.1.S1). An array-CGH analysis of four of the above five tumors showed reduction in the DNA copy number in those LOH regions (Fig. 2B), indicating interstitial and terminal

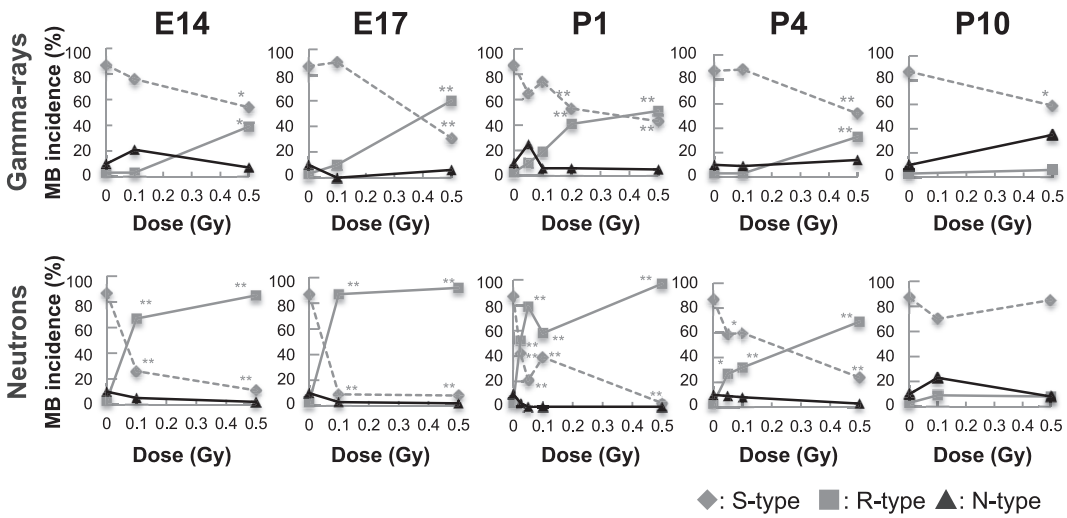

FIG. 3. Dose response of the incidence of S-, R- and N-type medulloblastomas in *Ptch1*$^{+/-}$ mice. *$P < 0.05$, **$P < 0.01$ vs. nonirradiated control by Fisher's exact probability test.

deletions of the C3H allele. Such patterns of LOH have not been observed in results from γ- and X-ray-induced tumors (*28, 29*).

Mutation of Ptch1 in MBs without LOH

In the above analysis, LOH encompassing the *Ptch1* locus was not detected in 53 of the 773 tumors (6.9%) [3 of 31 (9.7%) in the nonirradiated, 18 of 450 (4.0%) in the neutron irradiated, and 32 of 292 (10.9%) in the γ-ray irradiated groups], and we tentatively referred to these tumors as ''N-type'' (no evidence of LOH). Most MBs in *Ptch1*$^{+/-}$ mice show inactivation of the wild-type *Ptch1* allele, with only a minority retaining it intact (*34, 35*). We therefore analyzed the cDNA and genomic DNA of 37 N-type MBs (3 from nonirradiated, 12 from neutron irradiated, and 22 from γ-ray irradiated mice) and found mutations in *Ptch1* in 26 tumors (70%). MBs without any mutations in *Ptch1* were found only among the neutron- and γ-ray irradiated tumors and occurred at frequencies [6 of 12 (50%) and 5 of 22 (23%) N-type tumors, respectively] (Table 1 and Supplementary Fig. S4; https://doi.org/10.1667/RADE-21-00025.1.S1). Most of the mutations were deletions of 1–1,908 bp and resulted in *de novo* termination codons and amino acid changes affecting important functional sites including the Hedgehog-binding and sterol-sensing domains [3 of 3 (100%) N-type tumors in nonirradiated, 4 of 6 (67%) N-type tumors in neutron irradiated, and 9 of 17 (53%) N-type tumors in γ-ray irradiated mice]. Among them, the junctional sequences in five tumors (three in nonirradiated, one in neutron irradiated, and one in γ-ray irradiated mice) indicated that the deletions resulted from a DNA repair mechanism involving the microhomology-mediated end joining (Table 1 and Supplementary Fig. S4; https://doi.org/10.1667/RADE-21-00025.1.S1), a mechanism of mutagenesis not necessarily associated with radiation. The rest of the mutations were duplications, insertions, and base substitutions at splice acceptors, which also resulted in *de novo* termination codons and amino acid changes.

We further investigated whether the B6 or C3H alleles had the mutation for each tumor, taking advantage of SNPs and the *neo* cassette inserted in place of exons 6 and 7 in the B6 allele (Supplementary Fig. S1; https://doi.org/10.1667/RADE-21-00025.1.S1); these approaches enabled identification of the allele (i.e., B6 or C3H) harboring mutations in exons 3, 4, 9, 10, 21 and 22. The result showed that mutations were on the C3H allele, indicating that these mutations affected the function of the wild-type *Ptch1* allele, except for one case in the nonirradiated group that had a mutation in the B6 allele. Based on these results, the observed mutations in *Ptch1* in the ''N-type'' tumors were unlikely to be radiation specific. Furthermore, these N-type tumors did not increase in a dose-dependent manner, unlike the R-type tumors (Fig. 3). We therefore conclude that the N-type MBs should be classified as S-type, instead of R-type, tumors.

Assessment of the Effect of Gamma Rays and Neutrons on Induction of R-type MBs

Based on the above classification of MBs into S- and R-types, we analyzed the MB development after neutron and γ-ray irradiations at various ages relative to that of the nonirradiated group (Fig. 4A and Supplementary Fig. S5; https://doi.org/10.1667/RADE-21-00025.1.S1). The survival curves of mice with S-type MBs did not show significant differences between the nonirradiated and irradiated groups, except for a neutron irradiated group (0.5 Gy on P10) in which tumor development was decreased. As for the R-type MBs, neutrons significantly increased the tumor development at doses above 0.1 Gy in the E14 and E17 groups ($P < 0.05$), at or above 0.025 Gy in the P1 group ($P < 0.05$), and at 0.5 Gy in the P4 group ($P < 0.05$). Gamma rays also significantly increased tumor development at 0.5 Gy in the

TABLE 1
Mutations Identified in "N-type" Medulloblastomas

Radiation type, case no.	Age at irradiation	Dose (Gy)	cDNA alteration	Protein alteration	Junction (overlap sequence)	Exon(s) affected	Parental origin[a]
None							
1	N/A	0	c.2,662_2,845del	p. Leu888Ser fsTer917	MMEJ (TAGAC)	17	B6[a]
2	N/A	0	c.3,030_3,057del	p. Arg1,011Trp fsTer1,019	MMEJ (G)	18	n/d
3	N/A	0	c.2,783_2,792delinsA	p. Arg928Gln fsTer935	MMEJ (GGCC)	17	n/d
Neutrons							
4[b]	P4	0.05	c.353_542del	p. Val118Gly fsTer143	N/A	3	C3H[c]
5	P4	0.05	c.2,704delC	p. Pro902Arg fsTer910	N/A	17	n/d
6	P4	0.1	c.2,595delC	p. Asp865Glu fsTer889	N/A	16	n/d
7	P10	0.1	c.2,576_2,609dupinsA	p. Try859Ter	N/A	16	n/d
8	P10	0.1	c.1,362_1,385del	p. Val455_Leu462 del	MMEJ (GT)	10	C3H[c]
9	P10	0.1	c.2,726T>C	p. Leu909Pro	N/A	17	n/d
γ rays							
10	P1	0.05	c.2,600_2,604dup	p. Val867Gly fsTer887	N/A	16	n/d
11	P1	0.05	c.2,730delC	p. Thr910Thr fsTer918	N/A	17	n/d
12	P1	0.05	c.554delT	p. Leu185Trp fsTer206	N/A	4	C3H[c]
13[d]	P1	0.1	c.1,173_1,306del	p. Val392_Met435 del	N/A	9	C3H[c]
14	P1	0.2	c.2,731_2,734dup	p. Ala911 Ter	N/A	17	n/d
15	P1	0.5	c.3,240_3,251dup	p. Val1,080Thr1,083dup	N/A	19	n/d
16	P4	0.1	c.2,731_2,741del	p. Ala911Gln fsTer934	N/A	17	n/d
17	P4	0.1	c.2,679_2,681delinsAC	p. Leu893Leu fsTer909	N/A	17	n/d
18	P4	0.1	c.1,384_1,391dup	p. Ala464Ala fsTer479	N/A	10	n/d
19	P4	0.5	c.1,363del	p. Val455Trp fsTer477	N/A	10	n/d
20	P4	0.5	c.2,718_2,729dup	p. Thr910Thr fsTer929	N/A	17	n/d
21	P10	0.5	c.3,407_3,763del	p. Arg1,136Arg fsTer1,148	N/A	21, 22	C3H[e]
22	P10	0.5	c.2,704delC	p. Pro902Arg fsTer910	N/A	17	n/d
23	P10	0.5	c.2,792delG	p. Arg931Arg fsTer946	N/A	17	n/d
24	P10	0.5	c.2,710_2,716dup	p. Tyr906Cys fsTer941	N/A	17	n/d
25[f]	P10	0.5	c.1,305_1,306ins TTCTGCTTGCAG	p. Met435_Leu436insPheCysLeuGln		10	C3H[c]
26	P10	0.5	c.2,708_2,720del	p. Phe903Trp fsTer1,043	MMEJ (CGCTT)	17	n/d

Note. Reference sequences are NM_008957 (cDNA) and NP_032983.1 (protein). fs = frameshift; MMEJ = microhomology-mediated end joining; N/A = not applicable; n/d = not determined; P = postnatal.

[a] This cDNA lacked the sequence corresponding to exon 17; sequencing of genomic DNA from exons 16 to 18 identified a deletion of 1,183 bp that includes exon 17. The parental origin of the deleted allele was identified using five single-nucleotide polymorphisms (SNPs) in the introns.

[b] This cDNA lacked the sequence corresponding to exon 3. Genomic DNA was not analyzed because the length of the genomic DNA from exon 2 to 4 was too long (18,579 bp).

[c] The parental origin of mutation in exons 3, 4, 9 and 10 was identified using the sequence of exons 5 and 6, the latter of which is the site of insertion of the *neo* cassette.

[d] This cDNA lacked the sequence corresponding to exon 9; sequencing of genomic DNA around exon 9 indicated an intronic g-to-c transversion at the splice acceptor.

[e] This cDNA lacked the sequence corresponding to exons 21 and 22; sequencing of genomic DNA from exons 20 to 23 identified a deletion of 1,908 bp including exons 21 and 22. The parental origin of the deleted allele was identified using three SNPs in the exon.

[f] Sequencing of genomic DNA around exon 10 identified an intronic c-to-a transition at 12 bp upstream of exon 10, creating a new splice acceptor. As a result, the incorporation of 12 intronic base pairs into the cDNA affected the sterol-sensing domain of PTCH1.

E14 and E17 groups (both $P < 0.05$) and at or above 0.2 Gy in the P1 group ($P < 0.05$). Development of R-type MBs was strikingly suppressed in neutron- and γ-ray irradiated P10 groups. These results indicate that the age of susceptibility to radiation-induced MBs is confined to a period immediately after birth and is independent of the radiation quality used in these experiments. More importantly, the use of molecular subtypes enables distinction of radiation-induced tumors from spontaneous ones and thus allows quantification of the small effects of γ rays.

Finally, we analyzed the hazard ratio of R-type MBs for all experimental groups. The hazard ratio of all irradiated groups sharply increased in a dose-dependent manner except for the P10 groups (Fig. 4B), indicating that the R-type tumor is a useful indicator of radiation carcinogenesis. We therefore calculated the RBE of neutrons, relative to γ rays, based on the slopes of the dose response of R-type tumors (Fig. 4C); the P10 groups were not included, as R-type MBs did not increase in these groups. The RBE was calculated to be 12.9 (8.6, 17.2), 9.6 (6.9, 12.3), 21.5 (17.2, 25.8) and 7.1 (4.7, 9.5) (mean and 95% confidence interval) in the E14, E17, P1 and P4 groups, respectively (Fig. 4C). The confidence interval at P1 did not overlap those at other ages. Thus, the RBE of neutrons at P1 was highest and related to the susceptibility to radiation-induced tumorigenesis of the tissue.

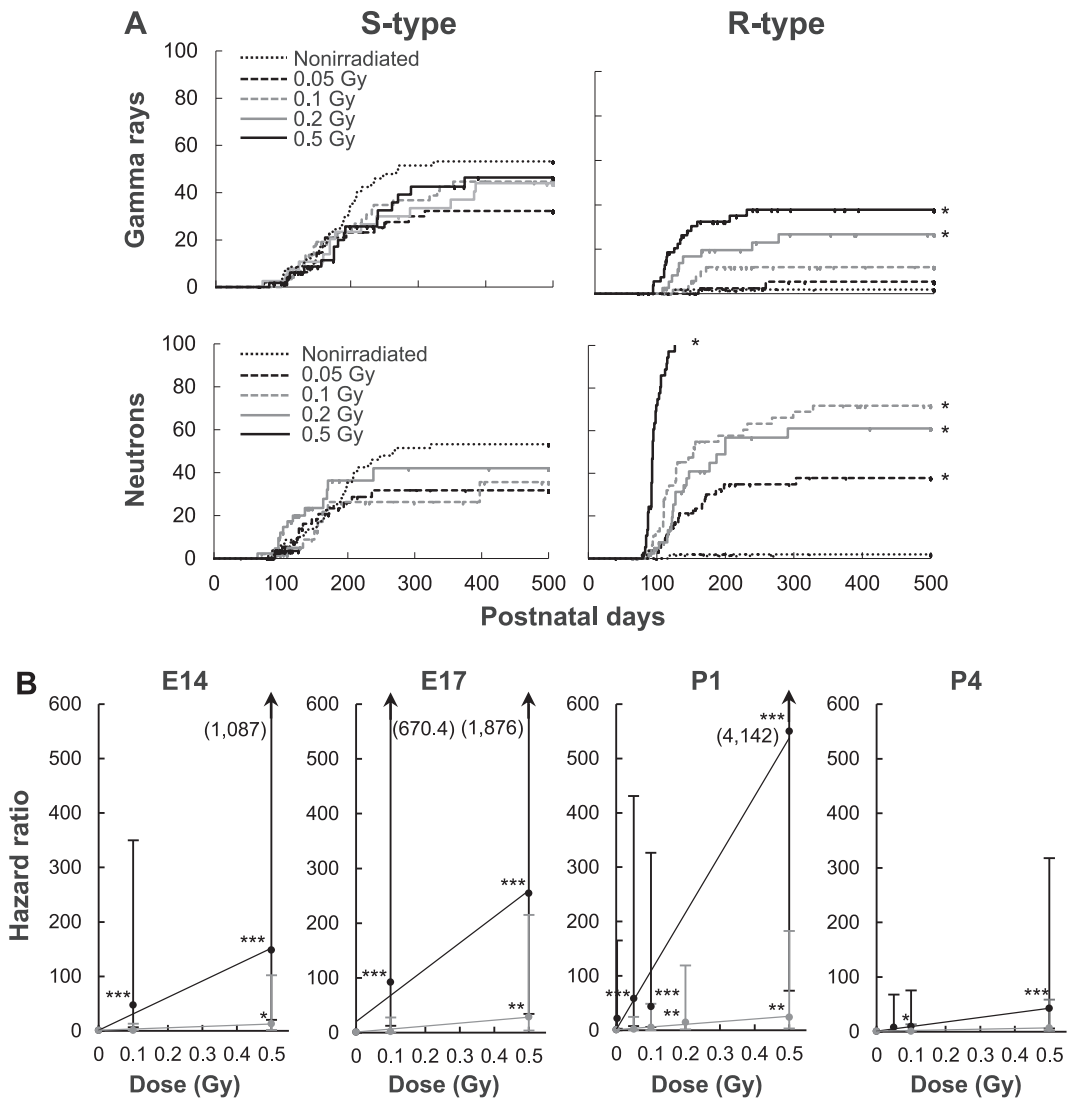

C

Age at exposure	Slope (95% CI) Gamma rays	Neutrons	RBE (95% CI)
E14	23.3 (16.2, 30.3)	301.0 (255.1, 346.9)	12.9 (8.6, 17.2)
E17	54.2 (43.4, 65.0)	522.9 (414.3, 631.5)	9.6 (6.9, 12.3)
P1	49.9 (41.8, 57.9)	1,072.9 (942.4, 1,203.1)	21.5 (17.2, 25.8)
P4	11.9 (8.2, 15.6)	84.2 (77.7, 90.7)	7.1 (4.7, 9.5)

FIG. 4. Incidence of R-type medulloblastomas and the relative biological effectiveness (RBE) of neutron calculated thereby. Panel A: Kaplan-Meier plots for the incidence of S- and R-type MBs in mice irradiated at P1. The data for 0.1 and 0.5 Gy of γ rays and for nonirradiated mice are reproduced from our previously published study (*29*). *$P < 0.01$ vs. nonirradiated group by log-rank test. Panel B. Dose response of the hazard ratio for R-type MBs in neutron- and γ-ray irradiated groups (black and gray, respectively). Hazard ratios for 0.1 and 0.5 Gy of γ rays were calculated using previously published data (*29*). The dose-response curves are fitted by linear equations. *$P < 0.05$, **$P < 0.01$ and ***$P < 0.001$ by Cox regression. Error bars indicate 95% confidence intervals; vertical arrows with a number in parentheses indicate the upper limit. Panel C: Slope of the linear equations in panel B and the RBE of neutrons. CI = 95% confidence interval.

DISCUSSION

The age at exposure is an important modifier of various radiation effects including carcinogenesis (*10*). Radiation exposure is more harmful to and more carcinogenic in infants than adults. The data presented herein show an age dependence for MB induction by fast neutrons in *Ptch1*$^{+/-}$ mice from E14 to P10, providing evidence consistent with two previously published studies reporting variation in the

RBE of fast neutrons based on the age at exposure (*19, 20*). An advantage of the current study over previous ones is its use of radiation-specific genetic aberrations in the tumor, i.e., interstitial deletions affecting the wild-type *Ptch1* allele as revealed by LOH and genomic copy number analyses. We found that 6.9% of MBs did not have LOH of chromosome 13 (designated as N-type) across the experimental groups, and most of these tumors had frameshift mutations in the functional domains of the wild-type *Ptch1* allele, resulting in *de novo* termination codons and amino acid changes. These mutations are similar to those observed by Frappart *et al*. (*36*) in mice with neural-tissue-specific inactivation of DNA double-strand break repair proteins combined with *Trp53* deficiency. MBs in those mice had lost one copy of *Ptch1* through chromosomal loss or translocation, and the remaining *Ptch1* allele contained mutations resembling those in the N-type tumors herein. We have also reported that $Tsc2^{Eker/+}$ rats, which have a mutation in a renal tumor suppressor gene, develop radiation-induced and spontaneous renal tumors exhibiting *de novo* termination codons in the wild-type *Tsc2* allele due to small deletions (*37*). Thus, these types of mutations, including those observed herein in the N-type tumors of $Ptch1^{+/-}$ mice, are not necessarily related to radiation exposure.

The susceptibility to radiation-induced carcinogenesis in $Ptch1^{+/-}$ mice was highest during the perinatal period (E14 to P1) regardless of the radiation type (i.e., both γ rays and neutrons) (Fig. 3 and 4, Supplementary Figs. S5; https://doi.org/10.1667/RADE-21-00025.1.S1), consistent with previously published studies in which the narrow age range of susceptibility was not affected by differences in radiation quality (*26, 28*). To evaluate the influence of age at exposure on carcinogenesis induced by radiation of different quality, it is crucial to extend the research to different animal models in which the age has a critical impact on carcinogenesis of organs relevant to radiological protection (e.g., bone marrow, liver, digestive tract and mammary gland). In particular, it would be ideal to use animal models that can distinguish radiation-induced tumors from spontaneous ones like those in $Ptch1^{+/-}$ mice.

The RBE of neutrons herein ranged from approximately 7 to 21 depending on the age at exposure, which overlaps the previously reported ranges of 5–8 for all malignant tumors and hepatocellular carcinoma in B6 mice (*19*) and 7–26 for mammary carcinoma in Sprague-Dawley rats (*20*); high-RBE values have generally been noted to be consistent with the age of high susceptibility to radiation carcinogenesis. A limitation of the current study is the relatively small number of dose points. The dose response of radiation induction of tumor is either non-linear (e.g., downward concave or convex) or linear in previously published studies (*19, 20, 38*), and RBE is greatly influenced by the shape of dose response. The current study is designed to have only two to five dose points, precluding the assessment of the shape of dose response. Nevertheless, the uncertainty resulting from this issue is evaluated as the confidence interval of the RBE value in the current study. An implication of the study is that the RBE value is age dependent and within the range of those reported previously. The current methodology is considered to offer more accuracy than previous studies in that it counts tumors most likely caused by radiation; thus, the result of the current study supports the conservativeness of the radiation weighting factor of neutrons, which is a function of energy having a maximum of 20, as recommended by the International Commission on Radiological Protection (*39*).

Although rare, we observed some (1.6%) neutron-induced MBs that had multiple deletions on chromosome 13, in which telomeric regions were affected by interstitial or terminal deletions in addition to the interstitial regions harboring the *Ptch1* gene (Fig. 2B). Cases with such coexisting deletions have not been reported in X- or γ-ray-induced tumors of $Ptch1^{+/-}$ mice. Interestingly, Brown *et al*. have also identified such types of complex deletions on chromosome 2 in a very small number of fast neutron-induced cases of acute myeloid leukemia in mice (*40*). These deletions are most likely a consequence of the biophysical nature of the interaction of neutrons with DNA. Fast neutrons produce high-LET recoil protons and α particles in the absorbing tissue, contributing to dense ionization and excitation of DNA molecules, thereby generating clusters of DNA damage, which are difficult to repair (*41–43*). These clusters of damage are likely to lead to a spectrum of mutations such as large deletions, translocations and other chromosomal aberrations (*43*), suggesting that the multiple deletions detected in neutron-induced MBs herein reflect the biophysical characteristics of fast neutrons. Three of five tumors with such multiple deletions developed postirradiation at P10 (Supplementary Fig. S3; https://doi.org/10.1667/RADE-21-00025.1.S1), a period of very low susceptibility as cerebellar granule cells have undergone substantial differentiation by this time (*26*). The mechanism of development of MBs via multiple deletions during this period of insusceptibility remains an issue for future work.

In conclusion, the age dependence of radiation induction of MBs in $Ptch1^{+/-}$ mice was not affected by radiation quality. The RBE of neutrons was evaluated based on the incidence of tumors harboring genetic aberrations that are most probably the direct consequence of radiation. Multiple deletions observed in some neutron-induced tumors are most likely related to a biophysical characteristic inherent to neutron radiation.

SUPPLEMENTARY INFORMATION

Table S1. Experimental groups and results of MBs development.

Table S2. *Ptch1* primers and PCR conditions.

Table S3. Primers for sequencing.

Fig. S1. Structure of mouse *Ptch1* and location of primers used for mutation analyses. Panel A: Genomic DNA (upper)

and cDNA (lower) of wild-type *Ptch1*. Topological domains (thick lines), which include glycosylation sites (triangles) and the sterol-sensing domain (dashed double-headed arrows), are indicated above the cDNA. The cDNA was divided into four segments (dashed lines with numbers) in the sequence analysis. Arrows flanking each segment indicate the primers listed in Supplementary Table S2. Panel B: Relevant exons of knockout (B6) and wild-type (C3H) alleles of *Ptch1*. Exons 6 and 7 in the genome are replaced by a neomycin resistance cassette. Dashed line reproduces segment 1 in panel A. Primers ''B6_F'' and ''B6_R'' were designed to sequence the B6 allele, whereas primers ''C3H_F'' and ''C3H_R'' are for the C3H allele. Primers ''B6_R'' and ''C3H_R'' were designed to analyze exons 3 and 4 of cases no. 4 and 12 (see Table 1), and primers ''B6_F'' and ''C3H_F'' were designed to analyze exons 9 and 10 of cases no. 8, 13 and 25 (see Table 1). Panel C: Primers for genomic sequencing to identify the cause of exon 17 deletion in cDNA from case no. 1. A 4,163-bp region between exons 16 and 18 (dashed line) was first amplified and then sequenced using primers referred to by the bracketed numbers. Alleles were identified using the two single-nucleotide polymorphisms (SNPs, triangles). Panel D: Primers for genomic sequencing to identify the cause of deletion of exons 21 and 22 in cDNA from case no. 21. A 6,167-bp region from exons 20 to exon 23 (dashed line) was first amplified and then sequenced using primers referred to by the bracketed numbers. Alleles were identified using the three SNPs (triangles).

Fig. S2. MB-free Kaplan-Meier plots after γ rays and neutron irradiation. $*P < 0.01$, $**P < 0.05$ vs. nonirradiated group by log-rank test.

Fig. S3. Loss of heterozygosity (LOH) of chromosome 13 in medulloblastomas from nonirradiated and neutron- and γ-ray irradiated groups. Panel A: Nonirradiated and neutron irradiated groups. Panel B: γ-ray irradiated group. Chromosomal regions and positions of polymorphic markers are shown on the upper left side in the schematic in panel A. Open circles indicate loss of the C3H allele, and filled circles indicate retention of both the B6 and C3H alleles. Results obtained for consecutive markers for individual MBs are aligned vertically; ''×'' indicates unavailable results. S-type or S = LOH in all consecutive markers distal to *Ptch1*; R-type or R = LOH confined to interstitial markers (big circles) or a polymorphism at position 4,016 in exon 23 of *Ptch1* (small circles); N-type or N = no evidence of LOH; ''No'' indicates tumors that were unavailable for LOH analysis. The numbers at the top of each column indicate the number of MBs with each LOH pattern. *These MBs showed multiple stretches of LOH.

Fig. S4. Mutations detected in *Ptch1* of medulloblastomas. Panels A–C: Characterization of mutations in MBs from nonirradiated (panel A), neutron irradiated (panel B), and γ-ray irradiated (panel C) mice. Sequences of the wild-type allele (upper) and identified mutations (lower) are indicated along with schematics for the relevant region of the cDNA (right-side bottom), in which solid boxes indicate exons, dashed boxes indicate deleted exons, and arrowheads indicate mutation sites. Numbers in the upper left side of each panel indicate the case number (see Table 1). Upper- and lowercase letters represent exonic and intronic sequences, respectively. Letters in blue = insertions; in green = duplications; in orange = base substitutions; in red = microhomology presumably used in end joining, which generated the deletion.

Fig. S5. Kaplan-Meier plots for the incidence of S- and R-type medulloblastomas. Separate graphs are shown for γ-ray irradiated and neutron irradiated groups. Plotted are the ages at death or moribundity of mice with MBs that were retrospectively determined to be S- or R-type; N-type tumors were treated as S-type. Data for mice irradiated with γ rays at E14 (0.1 and 0.5 Gy) and E17 (0.1 and 0.5 Gy) and P1 (0.1 and 0.5 Gy) and P4 (0.1 and 0.5 Gy) and for the nonirradiated group were reproduced from a previously reported study (*29*). Plots for the P1 group are the same as in Fig. 3. $*P < 0.01$, $**P < 0.05$ vs. nonirradiated group by log-rank test.

ACKNOWLEDGMENTS

We thank the Laboratory Animal and Genome Sciences Section, QST-NIRS, for animal facility management. We thank Drs. T. Imaoka and S. Kodaira for their helpful advice and discussion. This investigation was supported in part by a Grant-in-Aid for Scientific Research (C) from the Ministry of Education, Culture, Sports, Science and Technology (grant no. JP24700956) and QST Diversity Promotion Grant. Part of this work was conducted in association with the Joint-use Research Facility for Collaborative Project with NIRS-NASBEE.

Received: February 4, 2021; accepted: May 6, 2021; published online: May 27, 2021

REFERENCES

1. Badhwar GD, Keith JE, Cleghorn TF. Neutron measurements onboard the space shuttle. Radiat Meas 2001; 33:235–41.
2. Nishimura Y, Takeda H, Miyamoto K, Watanabe Y, Kouno F, Kuroda N, et al. Determination of 32P in urine for early estimation of the neutron exposure level for three victims of the JCO criticality accident. J Radiol Prot 2002; 22:25–9.
3. Howell RM, Ferenci MS, Hertel NE, Fullerton GD, Fox T, Davis LW. Measurements of secondary neutron dose from 15 MV and 18 MV IMRT. Radiat Prot Dosimetry 2005; 115:508–12.
4. Yonai S, Furukawa T, Inaniwa T. Measurement of neutron ambient dose equivalent in carbon-ion radiotherapy with an active scanned delivery system. Radiat Prot Dosimetry 2014; 161:433–6.
5. De Saint-Hubert M, Saldarriaga Vargas C, Van Hoey O, Schoonjans W, De Smet V, Mathot G, et al. Secondary neutron doses in a proton therapy centre. Radiat Prot Dosimetry 2016; 170:336–41.
6. Covelli V, Coppola M, Di Majo V, Rebessi S, Bassani B. Tumor induction and life shortening in BC3F1 female mice at low doses of fast neutrons and X rays. Radiat Res 1988; 113:362–74.
7. Maisin JR, Wambersie A, Gerber GB, Mattelin G, Lambiet-Collier M, De Coster B, et al. Life-shortening and disease incidence in C57BI mice after single and fractionatedy and high-energy neutron exposure. Radiat Res 1988; 113:300–17.
8. Broerse JJ, van Bekkum DW, Zoetelief J, Zurcher C. Relative

biological effectiveness for neutron carcinogenesis in monkeys and rats. Radiat Res 1991; 128:S128–35.

9. Warenius HM, Britten RA, Peacock JH. The relative cellular radiosensitivity of 30 human in vitro cell lines of different histological type to high LET 62.5 MeV (p–>Be+) fast neutrons and 4 MeV photons. Radiother Oncol 1994; 30:83–9.
10. Preston DL, Ron E, Tokuoka S, Funamoto S, Nishi N, Soda M, et al. Solid cancer incidence in atomic bomb survivors: 1958–1998. Radiat Res 2007; 168:1–64.
11. Mizumoto M, Oshiro Y, Yamamoto T, Kohzuki H, Sakurai H. Proton beam therapy for pediatric brain tumor. Neurol Med Chir 2017; 57:343–55.
12. Ohno T, Okamoto M. Carbon ion radiotherapy as a treatment modality for paediatric cancers. Lancet Child Adolesc Health 2019; 3:371–2.
13. Hall EJ. The impact of protons on the incidence of second malignancies in radiotherapy. Technol Cancer Res Treat 2007; 6:31–4.
14. Brenner DJ, Hall EJ. Secondary neutrons in clinical proton radiotherapy: a charged issue. Radiother Oncol 2008; 86:165–70.
15. Newhauser WD, Durante M. Assessing the risk of second malignancies after modern radiotherapy. Nat Rev Cancer 2011; 11:438–48.
16. Trott KR. Special radiobiological features of second cancer risk after particle radiotherapy. Phys Med 2017; 42:221–7.
17. Cordova KA, Cullings HM. Assessing the relative biological effectiveness of neutrons across organs of varying depth among the atomic bomb survivors. Radiat Res 2019; 192:380–7.
18. Preston DL, Cullings H, Suyama A, Funamoto S, Nishi N, Soda M, et al. Solid cancer incidence in atomic bomb survivors exposed in utero or as young children. J Natl Cancer Inst 2008; 100:428–36.
19. Maisin JR, Gerber GB, Vankerkom J, Wambersie A. Survival and diseases in C57BL mice exposed to X rays or 3.1 MeV neutrons at an age of 7 or 21 days. Radiat Res 1996; 146:453–60.
20. Imaoka T, Nishimura M, Daino K, Hosoki A, Takabatake M, Kokubo T, et al. Age modifies the effect of 2-MeV fast neutrons on rat mammary carcinogenesis. Radiat Res 2017; 188:419–25.
21. Imaoka T, Nishimura M, Daino K, Takabatake M, Moriyama H, Nishimura Y, et al. Risk of second cancer after ion beam radiotherapy: insights from animal carcinogenesis studies. Int J Radiat Biol 2019; 95:1431–40.
22. Harvard report on cancer prevention. Volume 1: Causes of human cancer. Cancer Causes Control 1996; 7:S3–59.
23. Taipale J, Beachy PA. The Hedgehog and Wnt signalling pathways in cancer. Nature 2001; 411:349–54.
24. Hahn H, Wojnowski L, Zimmer AM, Hall J, Miller G, Zimmer A. Rhabdomyosarcomas and radiation hepersensitivity in a mouse model of Gorlin syndrome. Nature 1998; 4:619–22.
25. Romer J, Curran T. Targeting medulloblastoma: small-molecule inhibitors of the Sonic Hedgehog pathway as potential cancer therapeutics. Cancer Res 2005; 65:4975–8.
26. Pazzaglia S, Tanori M, Mancuso M, Rebessi S, Leonardi S, Di Majo V, et al. Linking DNA damage to medulloblastoma tumorigenesis in patched heterozygous knockout mice. Oncogene 2006; 25:1165–73.
27. Pazzaglia S, Tanori M, Mancuso M, Gessi M, Pasquali E, Leonardi S, et al. Two-hit model for progression of medulloblastoma preneoplasia in Patched heterozygous mice. Oncogene 2006; 25:5575–80.
28. Ishida Y, Takabatake T, Kakinuma S, Doi K, Yamauchi K, Kaminishi M, et al. Genomic and gene expression signatures of radiation in medulloblastomas after low-dose irradiation in Ptch1 heterozygous mice. Carcinogenesis 2010; 31:1694–701.
29. Tsuruoka C, Blyth BJ, Morioka T, Kaminishi M, Shinagawa M, Shimada Y, et al. Sensitive detection of radiation-induced medulloblastomas after acute or protracted gamma-ray exposures in Ptch1 heterozygous mice using a radiation-specific molecular signature. Radiat Res 2016; 186:407–14.
30. Wilkinson P, Sengerova J, Matteoni R, Chen CK, Soulat G, Ureta-Vidal A, et al. EMMA–mouse mutant resources for the international scientific community. Nucleic Acids Res 2010; 38:D570–6.
31. Takada M, Suda M, Kamada S, Hagiwara T, Imaseki H, Hamano T. Neutron Exposure Accelerator System for Biological Effect Experiments (NASBEE). Application of Accelerators in Research and Industry 2011; 1336:401–5.
32. Morioka T, Blyth BJ, Imaoka T, Nishimura M, Takeshita H, Shimomura T, et al. Establishing the Japan-Store house of animal radiobiology experiments (J-SHARE), a large-scale necropsy and histopathology archive providing international access to important radiobiology data. Int J Radiat Biol 2019; 95:1372–7.
33. Kanda Y. Investigation of the freely available easy-to-use software 'EZR' for medical statistics. Bone Marrow Transplant 2013; 48:452–8.
34. Ayrault O, Zindy F, Rehg J, Sherr CJ, Roussel MF. Two tumor suppressors, p27Kip1 and patched-1, collaborate to prevent medulloblastoma. Mol Cancer Res 2009; 7:33–40.
35. Tamayo-Orrego L, Wu CL, Bouchard N, Khedher A, Swikert SM, Remke M, et al. Evasion of cell senescence leads to medulloblastoma progression. Cell Rep 2016; 14:2925–37.
36. Frappart PO, Lee Y, Russell HR, Chalhoub N, Wang YD, Orii KE, et al. Recurrent genomic alterations characterize medulloblastoma arising from DNA double-strand break repair deficiency. Proc Natl Acad Sci U S A 2009; 106:1880–5.
37. Inoue T, Kokubo T, Daino K, Yanagihara H, Watanabe F, Tsuruoka C, et al. Interstitial chromosomal deletion of the tuberous sclerosis complex 2 locus is a signature for radiation-associated renal tumors in Eker rats. Cancer Sci 2020; 111:840–8.
38. Ullrich RL, Jernigan MC, Cosgrove GE, Satterfield LC. The influence of dose and dose rate on the incidence of neoplastic disease in RFM mice after neutron irradiation. Radiat Res 1976; 68:115–31.
39. The 2007 Recommendations of the International Commission on Radiological Protection. ICRP Publication 103. Ann ICRP 2007; 37.
40. Brown N, Finnon R, Manning G, Bouffler S, Badie C. Influence of radiation quality on mouse chromosome 2 deletions in radiation-induced acute myeloid leukaemia. Mutat Res Genet Toxicol Environ Mutagen 2015; 793:48–54.
41. Nikjoo H, O'Neill P, Wilsonb WE, Goodheada DT. Computational approach for determining the spectrum of DNA damage induced by ionizing radiation. Radiat Res 2001; 156:577–83.
42. Georgakilas AG, O'Neill P, Stewart RD. Induction and repair of clustered DNA lesions: what do we know so far? Radiat Res 2013; 180:100–9.
43. Sage E, Shikazono N. Radiation-induced clustered DNA lesions: Repair and mutagenesis. Free Radic Biol Med 2017; 107:125–135.